Thermal interactions of the AD 79 Vesuvius pyroclastic density currents and their deposits at Villa dei Papiri (Herculaneum archaeological site, Italy)

Thermal interactions of the 79AD Vesuvius pyroclastic density currents and their deposits at Villa dei Papiri (Herculaneum archeological site, Italy)

Giordano G.*[1], Zanella E.[2], Trolese M.[1], Baffioni C.[1], Vona A.[1], Caricchi C.[3], De Benedetti A.A.[1], Corrado S.[1], Romano C.[1], Sulpizio R.[4], Geshi N. [5]

[1] Università Roma Tre, Largo San Leonardo Murialdo 1, 00146, Roma, Italia

[2] Università di Torino, Via Valperga Caluso 35, 10125 Torino, Italy

[3] Istituto Nazionale di Vulcanologia, Sezione di Roma 1, Via Vigna Murata 509, Roma, Italia

[4] Università di Bari, Via Edoardo Orabona, 4, 70126 Bari

[5] Geological Survey of Japan, AIST Site 7, 1-1-1 Higashi, Tsukuba, Ibaraki 305-8567, Japan

*corresponding author: email guido.giordano@uniroma3.it

Abstract. We studied the temperature of emplacement of pyroclastic density currents deposits that destroyed and buried the Villa dei Papiri, an aristocratic Roman edifice located just outside the Herculaneum city, during the 79AD plinian eruption of Mt Vesuvius (Italy). We used the Thermal Remanent Magnetization of lithic clasts embedded in the PDC deposits to retrieve accurate measures of the deposit temperature. The deposit shows substantial internal thermal disequilibrium. In areas affected by convective mixing with surface water or with collapsed walls, temperatures average at around 265°C (min 190°C, max 300°C). Where the deposits show no evidence of mixing with external material, the temperature is much higher, averaging at 350°C (min 300°C; max 440°C). Numerical simulations and comparison with temperatures retrieved at the very same sites from the reflectance of charcoal fragments indicate that such thermal disequilibrium can be maintained for time-scales well over 24-48 hours, i.e. the acquisition time for common

proxies of emplacement temperatures. We therefore reconstructed in detail the history of the progressive destruction and burial of Villa dei Papiri and infer that the deposit temperature is virtually the same as that of the incoming PDCs. This conclusion is very important as it solves a long standing debate on the actual relationships between the PDC deposit temperatures and those of the parent flows. Here we suggest that PDC deposit temperatures are excellent proxies for the temperatures of basal parts of PDCs close to their depositional boundary layer and therefore that mapping of deposit temperatures gives essential insights for thermal processes within PDCs and during their interaction with the affected environment.

1. Introduction

The main impact factors of pyroclastic density currents (PDCs) within their inundation areas are their temperature and dynamic pressure. While dynamic pressure is quantitatively related to the local momentum of the current (i.e. the instantaneous mass discharge over a certain area, e.g. a building; Dioguardi & Dellino, 2014), factors affecting the local temperature are much less understood. The general understanding is that, given an initial temperature of the pyroclastic mixture at vent (which largely depends on magma composition, possible interaction with ground- or crater lake-water, and amount of cold lithics excavated), the extent and efficiency of air ingestion during the collapse and ground hugging flow phases are the most effective ways for a pyroclastic density current to loose temperature, along with the entrainment of cold materials such as accidental lithics, vegetation, surface water and snow (see Paterson et al., 2010). However, the available dataset for temperature of pyroclastic flow deposits either directly measured or retrieved from various methods (Table S1 in Appendix 1) indicates that temperatures may vary

substantially and almost irrespectively of the PDC size, chemistry, lithic content, lithofacies (e.g. Cioni et al., 2004; Zanella et al., 2014; Pensa et al., 2015a). For example, ash clouds associated with confined pyroclastic density currents have been observed to leave behind thin and cold veneer deposits at Tungurahua 2006 (Eychenne et al., 2012) while similar occurrences were able to burn houses at Montserrat 1997 and Merapi 2010 (e.g. Jenkins et al., 2013). Similarly, thick valley pond ignimbrite deposits are known to vary from completely and laterally extensively welded (e.g. Willcock and Cas, 2014; Lavallée et al., 2015) to unwelded with T ranging from T > 600°C (e.g. Lesti et al., 2011) to low temperatures close to detection limits of common methods.

Given these uncertainties, much debate has fuelled the literature on defining the actual significance of temperature proxies measured in the deposits (e.g. McClelland and Druitt, 1989; Cioni et al., 2004; Paterson et al., 2010; Sulpizio et al., 2015; Zanella et al., 2014; Pensa et al., 2015a). The most used proxy is the Thermal Remanent Magnetization (TRM) of lithic clasts, and for example McClelland and Druitt (1989), Bardot (2000), Cioni et al. (2004) and Zanella et al. (2007) made a distinction between the temperature of pyroclastic flows and that of their deposits. Based on the longer time required for thermal equilibration of lithics respect to their residence in the flow, TRM-derived T are commonly interpreted as reflecting the deposit temperature rather than that of the parent flow.

Even longer is the equilibration time for charcolification of wood (Scott and Glasspool, 2005; Caricchi et al., 2014). Furthermore, by comparing the TRM on lithics and the degree of charcoalification of wood, Pensa et al (2015a,b) warned us about the complicated history of pre-heating of lithic clast which may be extracted anywhere from deep in the conduit, from the vent, or picked up along flow, all potentially carrying very different temperatures at their final landing.

Other important though rather poorly explored topic are: i) what is the relative contribution to the final temperature at deposition of the polycomponent and polydispersed pyroclastic

debris, and ii) how long it takes for the deposit to significantly depart from the temperature of the parent pyroclastic flow when compared with the characteristic time of thermal equilibration for the different proxies.

In this paper we analyse in detail the temperature of the pyroclastic flow deposits of the 79 AD eruption at Vesuvius which destroyed the city of Herculaneum during the evening-night between August 24 and 25. Unlike other previous works that approached the problem at a large scale (e.g., Zanella et al., 2014), we work to define the interaction over time of incoming PDCs with one building. We extend the dataset presented in Caricchi et al. (2014) which was only based on charcoal fragments and integrate with TRM analysis of lithics from many sites in and around the Roman Villa dei Papiri, across stratigraphy and different lithofacies. The presented dataset and a numerical modeling of the thermal behaviour of the deposit suggest that proxies for PDC deposit temperature largely record a disequilibrium temperature dominated by the ash fraction and that this temperature cannot be substantially different from that of the parent flow. Hence, with the exception of local effects associated with physical mixing with water or sediment or other external cold materials, the deposit temperature closely reflects the flow dynamic processes that determine the extent of heat loss of the ash fraction prior to deposition.

2. Summary of the 79 AD eruption and the deposits of Herculaneum excavations

The chronology of the 79 AD eruption is based on the accounts of Pliny the Younger and translated to processes and timing by Sigurdsson et al. (1982, 1985). The stratigraphy has been divided into 8 Eruption Units by Cioni et al. (1992, 1996, 2004). The stratigraphy in Herculeneum is described in Gurioli et al. (2002).

The eruption started on August 24 at around noon with a not better specified phreatomagmatic event (EU1: phreatomagmatic ash). At around 1PM a buoyant column

106 rose up to 30-33 km high (Carey and Sigurdsson, 1987) producing stratified SE-ward-
107 dispersed fall deposits. The first pulse lasted till around 8PM (EU2f phonolitic white pumice
108 lapilli) and the second across the night (EU3f phonotephritic grey pumice lapilli). During
109 this early phase, partial collapses produced the pyroclastic flows (EU2/3pf and EU3pf) that
110 reached Herculaneum (Barberi et al., 1989; Cioni et al., 2000a,b).
111 During the following day, on August 25th, the onset of the caldera collapse eventually led to
112 the generation of radially spreading pyroclastic flows (EU4-5-6-7; Cioni et al., 2004; Gurioli
113 et al., 2007), with lithic rich breccias (EU6) and evidence for magma-water interaction
114 (Barberi et al., 1989; Cioni et al., 1992). The eruption ended with the deposition of a thick,
115 phreatomagmatic, accretionary lapilli-bearing ash (EU8).
116 According to the stratigraphy in Gurioli et al. (2002) and Caricchi et al. (2014),
117 Herculaneum did not receive the deposition of the initial pumice fallout, being cross-wind
118 respect to dispersal axis. The stratigraphic succession records the PDC deposits (E2/3pf;
119 EU3pf) associated with the partial collapses of the column during the transition between
120 phonolitic EU2 and phonotephritic EU3 phases, and later PDC deposits of the caldera
121 forming phase (EU4 to EU8).
122
123
124 **3. Previous works, materials and methods**
125
126 The stratigraphy and sedimentology of the 79 AD Vesuvius eruption deposits have been
127 studied in detail in several works including their temperature with various methods (e.g.
128 Lirer et al., 1973; Kent et al., 1981; Sigurdsson et al., 1982, 1985; Carey and Sigurdsson,
129 1987; Cioni et al., 1990, 1992, 1996, 2000a, 2000b; Yokoyama and Marturano,1997;
130 Mastrolorenzo et al., 2001; Gurioli et al., 2002, 2005; Caricchi et al., 2014).
131 Villa dei Papiri was an aristocratic Roman villa located just outside the main
132 Herculaneum city (Fig. 1a,b), along the 79 AD Roman coastline (Guidobaldi et al.,

2009) The Villa was reached by the early intra-plinian PDC and progressively buried and partially destroyed by the following PDCs which deposited more than 30 m of dominantly massive and chaotic lapilli tuff (Fig. 1c,d).

The temperature of the deposit that buried and destroyed the Villa dei Papiri is herein retrieved from the determination of the Thermal Remanent Magnetization (TRM) of the lithic clasts embedded in the lapilli tuff of units EU2/3pf, EU3pf, EU4 (Fig. 1c,d). Details on the method are given in Appendix 1. We sampled lithics in the size range of 1-3 cm ca taken from massive and chaotic facies (Appendix 2). Eight sites (VP1, VP2, VP5.1-3-5-7-10, VP9) were sampled where the ash matrix < 1mm represents > 75% of the deposit (Gurioli et al., 2002). Additional four sites were sampled were the deposit is fines-depleted within a large gas-pipe (VP8) within a strongly zeolitised facies (VP6), and where it is mixed with coarse debris from the collapse of the Villa (VP3, VP4). Four out of our twelve sampling sites (i.e. VP1, VP2, VP3, VP4) also correspond to the very same sites where emplacement temperatures had been previously interpreted from charcoal fragments in Caricchi et al. (2014). We devised this sampling strategy because charcoal equilibrates with the embedding deposits in timescales of 10^1 hours, usually 24 hours or more (Scott and Glasspool, 2005; Caricchi et al., 2014), while cm-sized lithics do so within much shorter timescales, usually < 10^0 hours (Bardot and McClelland, 2000; Cioni et al., 2004). By comparing TRM data and published charcoal data from the very same sites we aim therefore at appreciating the influence of thermal disequilibrium processes, such as those associated with the cooling of the deposit which may produce a significant departure of the recorded temperatures and those of the first arrival, as well as processes associated with the internal re-equilibration of temperatures carried by the poly-component and poly-dispersed pyroclastic material in its interaction with topography and infrastructures.

INSERT FIG. 1 HERE

4. Results

4.1 Thermal Remanent Magnetization of lithic clasts

The magnetization components of a lava fragment embedded in a PDC deposit reveal its thermal history. In a simplified model, if the lava fragment is re-heated after its formation, it shows two magnetization components: i) a high-T component, representing what remains of the TRM, originally acquired by the ferromagnetic grains in the lava throughout their blocking temperature (T_b) spectrum, and ii) a low-T component, result of the PDC re-heating process.

The analysis of the Zijderveld diagrams (Fig. 2) provides the magnetization components and the re-heating temperature (T_r) interval. For each of the 190 measured specimens we determined a T_r interval and classified the behavior during the demagnetization process into four different types (labeled A to D), as proposed by Cioni et al. (2004), on the base of the relation between specimen T_b spectrum and re-heating temperature (T_r). Details are given in Appendix 1. Here we just recall that, depending on the assemblage of magnetic grains within a clast, for two types (i.e. C and D) a heating interval is obtained. Instead, types A and B are characterized by one magnetization component, the primary high-T and the secondary low-T component, respectively. In both these cases it is not possible to get any information on the T_r.

The Zijderveld diagrams analysis provided successful results, i.e. a heating interval, in 72% of the total (Fig. 2). For type C, the T_r intervals were determined in a range of 40 °C (Fig. 2a, b); for type D, during demagnetization a clear curvilinear trend is displayed, as highlighted in Fig. 2c, and the T_r interval is wider, normally more than 80 °C. For the remaining, the 9% is represented by A (Fig. 2d) + B types, the 19% by unresolvable cases,

where the angle between the two magnetization components was <15° (Porreca, 2004). During thermal demagnetization, specimens mostly proved to have a high magnetic stability and no alteration, as evidenced by magnetic susceptibility variations, were detected.

All the lithics of site VP8 show three magnetization components, whose layout highlights two T_r intervals: one in the range 280-320 °C, the other in the range 160-200 °C. The former is fully consistent with the T_r intervals determined in all the other sampling sites; the latter represents the lowest T_r intervals within *Villa dei Papiri*.

INSERT FIG 2 HERE

Having determined all the T_r intervals, for each sampling site we prepared an overlapping diagram (Fig. 3): the temperature of the deposit T_{dep} is in the range where the greatest number of T_r intervals falls. This method has its main limit in the qualitative approach. Nevertheless, the fact that both the studied deposits and the lithic fragments are heterogeneous (no information is at priori available on the thermal history of the lava clasts and on their magnetic properties) reinforces the reliability of the results (Zanella et al., 2014). Besides, a statistical approach for T_{dep} estimation based on the Gaussian method has been recently applied to the Minoan eruptive deposits of Santorini (Tema et al., 2015). Results obtained from the mathematical method were fully consistent with those from the overlapping method. T_{dep} intervals are listed in Table 1. The T_{dep} varies from 180 to 440 °C with mean value ranging from 280-340 °C (Table 1). This range is fully consistent with the T_{dep} values already reported for the 79 AD deposits around Vesuvius (Cioni et al., 2004). The lowest interval is displayed in VP8, whose lithic clasts have been sampled in a gas-pipe.

INSERT FIG. 3 AND TABLE 1 HERE

212

213 *4.2 Interpretation of TRM data*

214

215 TRM data at Villa dei Papiri show quite a large variability ranging from 180°C to 440°C.
216 These data are consistent with previously published data on deposit temperature obtained
217 from charcoal fragments at the very same localities (Fig. 1; Table 1; cf. Caricchi et al.,
218 2014). We therefore trust the values obtained (cf. Pensa et al., 2015b) that need, though,
219 to be addressed for their variations in such a very limited area. These variations partly
220 reflect the stratigraphy, where the three sites sampled in lower unit EU2/3pf, VP4, VP6 and
221 VP8, show the lowest T_{dep} values (Fig. 1 and Table 1). In particular site VP8, with a T_{dep} of
222 180-200°C, was sampled within a large gas pipe generated by the interaction of the
223 incoming PDC with the sea shoreline (Fig. 4b and Appendix 2), while site VP6, with a T_{dep}
224 of 280-320°C, within the zeolitised halo around the pipe (Fig. 1d and Appendix 2), likely
225 generated by the upward percolation of vapourised seawater. Site VP4, with a T_{dep} of 260-
226 300°C, is instead sampled in a breccia facies made of mixed pyroclastic material and
227 debris from collapsed wall of the Villa (Fig. 4c and Appendix 2). At this site VP4 the
228 temperature from TRM of lithics is in perfect agreement with that retrieved by Caricchi et
229 al. (2014) from reflectance analysis of chacoal fragments embedded in the very same site
230 (Table 1). We interpret therefore the low values associated with EU2/3pf with a significant
231 interaction of the incoming PDCs with the environment, either seawater or the partially
232 destroyed Villa. Data from the upper units EU3pf and EU4 (VP1, VP2, VP5.1-3-7-10) are
233 on average much higher (Table 1) and indicate temperatures that are consistent with
234 maximum values reported in literature as characteristic of the 79 AD deposits outside
235 towns (Cioni et al., 2004; Zanella et al., 2007; 2014). Noticeable exceptions are sites VP3
236 and VP5.5. Site VP3 is located inside the building where the EU4 deposit is admixed with
237 collapsed walls (Fig. 4d and Appendix 2). Also for this site data from reflectance analysis of

chacoal fragments embedded in the very same site are available (Caricchi et al., 2014; Table 1) and match perfectly with our TRM data, so like for VP4 we interpret the lower temperatures in terms of cooling effect of the edifice debris. Site VP5.5 is instead somewhat problematic as it is far from the edifice and closely surrounded by sites characterised by much higher temperatures, so this may either be an outlier or a site affected by some cooling agent difficult to identify (e.g. a close gas pipe present in the third dimension but invisible along the exposed face where lithics had been sampled; Fig. 1c). In summary the average of the mean values obtained for each of the sites affected by evident cooling agents (VP4, VP6, VP8, VP3) gives a value of 265°C (Fig. 5). This temperature contrasts with a similar average for sites unaffected by evident cooling agents (VP1, VP2, VP5.1-3-5-7-10, VP9) where the value is 348°C (Fig. 5). It must be noticed that sites VP1, VP2 and VP5.1 are located at distances of less than 1 m from the intact Villa walls (Fig. 1c) and bear no edifice debris inside. This indicates that the presence of the Villa edifice was “felt” by the deposit in terms of heat transfer generating thermal disequilibrium at short time and length scales only where the collapsed walls physically mixed with the pyroclastic material, whereas in absence of physical mixing with cold debris, the pyroclastic deposit is very poorly affected by the temperature of the substrate. Similarly, the convective mixing with seawater is an efficient cooling agent for the PDC deposit.

INSERT FIG. 4 AND FIG. 5 HERE

5. Numerical Modeling

In order to better understand the time and length scales of the thermal interaction between PDC deposits and the Villa dei Papiri edifice we performed numerical simulations of the

burial of the Villa with the Heat3D software (Wohletz, 2008). We define a 3 m x 3 m computational domain with a 5 cm cell-grid. We computed the conductive heat transfer between the hot PDC deposits and the wall of the Villa at ambient temperature, as convection in the deposit can be disregarded. We defined two configurations (Fig. 6a,b): configuration A is aimed at simulating the contact between the vertical wall of the Villa and the PDC deposit within a distance of 2 m from the wall (e.g. VP1, VP2, VP5-1); configuration B is aimed at simulating the collapse of the wall and the mixing with the PDC deposit (e.g. VP3 and VP4). Table 2 shows the parameters used to characterise the building and the deposit physical properties.

INSERT TABLE 2 HERE

We simulate the PDC deposit as a continuum at the scale of simulation with a density of 1200 kg m^{-3} and thermal conductivity of 0.7 W m^{-1} K^{-1}, specific heat 1200 J kg^{-1} K^{-1} and initial T of 350°C, taken as the average of our data away from the building (from transect VP5) and in agreement with previous estimations. Time steps of the numerical solutions are determined by the dimension of the cells so that the minimum simulated is 15 minutes, lower than the time of acquisition of the TRM signal by the analysed lithics. Runs simulated 48 hours of thermal exchange between the ignimbrite and the Villa, that is longer than the time of acquisition for charcoal. We therefore are able to analyze the temperature variations in the deposit in a time-frame that encompasses the time-scales of acquisition for both proxies.

Results indicate that configuration A promotes very little heat transfer during the first 48 hrs, with a T drop of less than 50°C in the deposit at 50 cm distance from the contact with the wall and almost no variations at 1 m distance (Fig. 6c). This explains why the temperatures acquired by both the lithic and the charcoal proxies at sites even close to the

Villa (e.g. VP2) but where the structure did not collapse do record accurately the emplacement temperatures with very small departures from the initial values.

By contrast, results from configuration B (Fig. 6d) indicate that the mixing between a collapsed wall and the PDC deposit promotes a very fast and efficient heat transfer due to the enhanced contact surface available.

INSERT FIG. 6 HERE

Fig. 6d shows that the initial thermal disequilibrium, though highly simplified geometrically, rapidly smooths with a T drop of more than 100°C inside the PDC deposit domains in the first 3 hours of simulation and smooths to an average value of less than 200°C, that is more than 150°C less than initial, after 6 hours. At the same time, once re-equilibrated, the temperatures in the collapsed domain remain almost constant to the end of the simulation after 48 hours. Runs performed for configuration B with a finer cell-grid of 0.5 cm in a 30 cm x 30 cm domain (Appendix 3) indicate that the thermal equilibration occur within the first 15 minutes. These results explain the relatively similar and low T recorded by both lithic and charcoal at sites VP3 and VP4, i.e. where the PDC deposits are fully mixed with portion of collapsed walls of the Villa.

6. Discussion

What we know about thermal processes within pyroclastic density currents and their deposits is still rather vague. Current knowledge relies on a very limited number of direct measurements of deposit temperatures taken with thermocouples from the shallowest part of deposits when and where approachable, and a number of studies of the TRM of embedded lithic clasts and reflectance of charcoal (Table S1, in Appendix 1). Some of the main still open questions are: i) what is the actual relationship between the temperature of

317 the deposit and the temperature of the parent current; ii) what temperature is actually
318 recorded by commonly used deposit proxies, considering (a) the inherent thermal
319 disequilibrium of the poly-dispersed and poly-component pyroclastic material (b) the local
320 interaction with the environment and (c) the density and thermal stratification within PDCs.
321 Data from the Villa dei Papiri show that temperatures retrieved from TRM of lithic clasts
322 are in excellent agreement with temperatures derived from the reflectance of charcoal
323 fragments taken at the very same sites by Caricchi et al. (2014) (Table 1, Fig. 5). This
324 agreement indicates that temperatures in the deposit at each site remained stable for time-
325 scales comparable with the acquisition times for both proxies, i.e. for at least 24-48 hours.
326 These results are also in good agreement with numerical simulations, which show, within
327 48 hours, a substantial stability of the temperature close to initial values even very close to
328 a cold substrate, which in our case is the wall of the Villa (Fig. 6b). This is due to the low
329 thermal conductivity of glass shards and crystals that form the ash matrix, so that, in
330 absence of convective effects promoted for example by water vapourization or other kinds
331 of physical mixing with cold materials (e.g. collapsed intrastructures), the timescale of
332 deposit cooling is much longer than that required for equilibration of lithics and charcoal
333 fragments: this suggests that the values retrieved from our proxies record the deposit
334 temperature very close to that of emplacement. Our data therefore indicate that, in the
335 case of Villa dei Papiri, the highest measured temperatures away from areas of obvious
336 mixing of the deposit with either water (e.g. VP8) or collapsed walls (e.g. VP3, VP4)
337 represent not only the deposit temperatures but are very close to the emplacement
338 temperatures. We also notice that lithics sampled for our TRM analyses have been taken
339 from massive and chaotic lapilli tuff facies, where the ash fraction, both coarse and fine,
340 represents between 50 and 90%wt, with most common values >75%wt of the deposit
341 (Gurioli et al., 2002; Appendix 2). Available literature indicates that particles in the ash
342 fraction equilibrate almost instantaneously with the ambient (e.g. Wilson et al., 1978;

343 Thomas and Sparks, 1992). The ash fraction can therefore be assumed as continuously
344 thermally equilibrated within flow and at deposition. Possible sources of thermal
345 inhomogeneity (both as heat sources or heat sinks) in the deposit could therefore be
346 related to the presence of large lapilli or bomb sized clasts. Bomb sized clasts in the
347 primary 79 AD deposits at Villa dei Papiri are very rare and lapilli represent usually less
348 than 10-15%wt of the deposit. These proportions already suggest that the largest
349 contribution to the deposit temperature is provided by the ash fraction inside which the
350 lithics (and the charcoal measured in Caricchi et al., 2014) have been sampled. The
351 deposit temperatures retrieved from sites with no visible convective interaction with either
352 water or collapsed walls, though variable, all sit at the high-end of the thermal spectrum of
353 the deposits (> 300 °C) and strongly suggest a common origin, which we interpret as
354 provided by the ash matrix. If that is true, as we believe our data clearly indicate, than the
355 measured deposit temperature not only is very close to the emplacement temperature, but
356 also to the temperature of the basal and more concentrated part of the flow close to the
357 depositional boundary layer (sensu Branney and Kokelaar, 2002)(Fig. 7). We therefore
358 conclude that, close to their flow boundary layer, incoming PDCs at Herculaneum had a
359 bulk temperature > 300 °C and based on the most frequent values retrieved most likely
360 around 350 °C (Fig. 5), carried essentially by the most abundant ash fraction. This
361 conclusion is very important as it answers a long-standing debate on the actual
362 significance of the deposit temperature in respect to the parent flow. We suggest here that
363 the emplacement temperature of ash-matrix supported PDC deposits essentially reflects
364 that of the parent flow even very close to substrate (Fig. 7), as conductive cooling of the
365 deposit is much slower than the acquisition time for commonly used proxies, namely lithic
366 clasts and charcoal.
367 Based on the above considerations we propose a detailed reconstruction of the
368 destruction and burial of the Villa dei Papiri from the PDCs that stroke Herculaneum during

369 the evening and night between the 24 and the 25 of August 79AD (Fig. 8).
370 The first PDC that reached the Villa was EU2/3pf, i.e. the PDC that formed at the transition
371 between the two main sustained plinian phases EU2 and EU3 both SE-ward directed and
372 therefore not recorded at Herculaneum (Fig. 8a,c; Gurioli et al., 2002). The PDC was able
373 to unroof the Villa and partially destroy sections of it, but most of the main structure
374 remained in place. Debris mixed within EU2/3pf deposits at site VP4 relate to such event
375 (Fig. 8b). At the same time the PDC crossed the coastline just in front of the Villa, entered
376 the sea depositing and pushing forward the sea-shore (Fig. 8b). Deposit temperatures are
377 highly dishomogeneous (Table 1), with the lowest measured in this study (180-200°C) and
378 reflect rapid post-emplacement heat transfer processes of mixing with sea-water/vapour
379 and debris. Timescales of such processes are < 1 hour, i.e. the time-scale needed for 1-3
380 cm sized lithics to equilibrate with the embedding deposits (Cioni et al., 2004). After a
381 pause associated with the restoration of the EU3 buoyant plume which kept depositing
382 pumice fallout to the SE of the volcano (Fig. 8c), a second major PDC reached the Villa dei
383 Papiri site, EU3pf, which partly buried the still standing main edifice and invading most of
384 its interior (Fig. 8d). EU3pf however did not cause major collapses to the structure, nor it
385 interacted with the sea-water, previously buried by the EU2/3pf deposits. Deposit
386 temperatures in EU3pf average at around 350°C (Table 1 and Fig. 5) even within or very
387 close to the Villa (VP1, VP2), both from TRM data presented herein and from charcoal
388 data presented by Caricchi et al. (2014), and reflect the average temperature of the parent
389 PDC close to its depositional boundary layer (Fig. 7). The following PDC, EU4pf, reached
390 the Villa after the transition from the buoyant EU3 phase and the beginning of the caldera
391 collapse phase which was thereon dominated by PDCs (Fig. 8e,f). With the arrival of the
392 EU4 PDC the Villa was completely buried and the deposits are locally mixed with debris
393 from the collapsed walls of the summit floor that is totally unroofed (Fig. 8g). Based on the
394 highest temperatures retrieved in EU4 we interpret the parent PDC to have arrived in town

with a temperature just above 350°C close to its depositional boundary layer, that is similar to that of the previous EU3pf.

INSERT FIG. 7 AND FIG. 8 HERE

7. Conclusions

We have presented a detailed study of the temperature of the 79 AD PDC deposits that progressively destroyed and buried a large ancient Roman edifice, the Villa dei Papiri, at Herculeneum. We measured the TRM of lithic clasts embedded in the ash matrix of massive and chaotic facies and compared the results with temperatures retrieved from the reflectance of charcoal fragments collected at the very same sites by Caricchi et al. (2014). The excellent overlap between the two datasets allows to draw several important conclusions very relevant for our conceptual and physical understanding of pyroclastic density currents, as well as to reconstruct in detail the history of the thermal interaction between the incoming PDCs and the Villa dei Papriri edifice and its environment.

The main conclusions are:

1) The temperature of the ash-matrix supported, massive and chaotic PDC deposits remains stable over time-scales of 24-48 hours that encompass the different acquisition times for both TRM and charcoal proxies; this temperature stability suggests that the emplacement temperature of the ash-matrix, where unaffected by external factors (see point 2 below), cannot be substantially different from that of the deposit at the time of acquisition; in turn the temperature of the basal part of the current, close to its depositional boundary layer prior to deposition cannot be substantially different and we conclude that the deposit temperature is an excellent proxy for the temperature of the base of PDCs.

2) The temperature of PDC deposits is significantly and quickly affected by external factors across the acquisition times of TRM and charcoal proxies only where convective mixing occurs, either with external water, rock debris or else; such occurrences define local

thermal domains within the PDC deposits and their thermal disequilibrium with the surroundings can be maintained for time-scales much longer than 24-48 hours.

3) The reconstruction of the thermal interactions at Villa dei Papiri shows that the first incoming PDC had the largest degree of mixing with both debris from the unroofing of the edifice and partial collapses, along with the interaction with the sea facing the Villa; the following PDCs were thermally affected by the Villa only where collapsed occurred, otherwise the purely condictive thermal equilbration along standing walls takes much longer than 24-48 hours even at <50 cm from contact between PDC deposit and wall.

4) The average PDC deposit temperature at Villa dei Papiri is around 350°C, which we indicate as that of the parent PDCs. The significant drop from magmatic temperature (around 850 °C for fragmenting trachy-phonolitic magma; Cioni et al., 1995) could be due to a combination of eruptive (e.g. magma water interaction and/or air entrainment in the column during collapse) and flow processes (e.g. air/water/vegetation ingestion along flow). The substantial homogeneity of the temperatures obtained spatially for the 79 AD PDC deposits (Cioni et al., 2004), very simlar to all other PDC deposits along the history of Vesuvius (Zanella et al., 2014) suggest some common process that needs further investigations.

Acknowledgements

This work was funded by the DPC grant

Figure captions

Figure 1: a) location of Villa dei Papiri and Herculaneum respect to Vesuvius; b) detailed map of the Villa dei Papiri excavations and location of sampling sites; c,d) volcano-ward

448 and sea-ward views of the Villa dei Papiri archeological excavation and location of
449 sampling sites (VP) in relation with the stratigraphy of the 79 AD eruption. Temperature
450 ranges in blue indicate results from TRM of lithic clasts obtained in this study, compared
451 with values obtained from charcoal by Caricchi et al. (2014) indicated in red. White
452 numbers indicate elevations in m a.s.l. (photo and elevation survey courtesy of
453 Superintendence for Archaeology of Herculaneum).
454
455 Figure 2: Examples of the demagnetization results: Columns (left to right): (1) Normalized
456 intensity (J/J0) decay curve. The grey bar shows the re-heating range; (2) Zijderveld
457 (1967) diagram: solid/open dots represent declination/apparent inclination; figures
458 represent T values (°C). Red/blue line are the interpolated high-T and low-T magnetization
459 components, respectively; (3) Equal-area projection: solid/open dots represent lower/upper
460 hemisphere. Examples refer to type C (a) and (b), D (c) and A (d).
461
462 Figure 3: Deposition temperature at site VP6. The site Tdep is estimated from the
463 overlapping Tr ranges for
464 all lithic clasts sampled at this site. On the left, twin-specimens are limited by a square.
465 Frequency-histogram
466
467 Table 1: Site deposition temperature, Tdep (°C). Legend: n/N number of Tr interval in the
468 overlapping range out of number of measured lithic clasts; type A, B, C, D as in Cioni et al.
469 (2004). The question mark indicates the unresolvable Zjiderveld diagrams. Tchar indicates
470 temperatures retrieved by Caricchi et al. (2014) from the analysis of the reflectance of
471 charcoal fragmants sampled at the very same sites.
472
473 Figure 4: a) plan view of sampling sites (see also Fig. 1); b) detail of the large gas pipe

affecting EU2/3 ; c) basement floor of the Villa where the EU2/3 ignimbrite is both mixed with collapsed debris and affected by sea-water mixing; d) third floor of the Villa where the EU4 ignimbrite is partly mixed with collapsed debris; data in red (and in (c)) are from Caricchi et al. (2014).

Figure 5: Deposit temperature at each measured site (see Fig. 1 for location). Open circle indicate the mean values for TRM samples and bars the related T interval; Red bars indicate temperatures retrieved from charcoal reflectance from Caricchi et al (2014). The average of undisturbed and mixed facies are given by dashed lines.

Table 2: Physical properties of rocks used for the simulation in Heat3D (from Turcotte and Schubert, 2014; Eppelbaum et al., 2014).

Figure 6: Main results of the Heat3D numerical modeling of heat transfer between the ignimbrite (red domain) and the wall (blue domain) for the two chosen configurations at t=0: A is the intact wall; B is the collapsed wall mixed with the ignimbrite; the cell-grid is 5 cm. Diagrams below each initial configuration show the temperature evolution over 24 hours taken along the green line.

Figure 7: Cartoon illustrating the different thermal interactions of the incoming PDC with the environment, which promote rapid changes of temperature of the deposit in different though very close settings. Note that T°C at the base of the incoming PDC is everywhere ~350°C, similar to that of the deposit unless mixing with either debris or water occurs during emplacement.

Figure 8: Reconstruction of the progressive destruction and burial of the Villa dei Papiri;

500 stratigraphic units according to Gurioli et al. (2002); chronology according to Sigurdsson et
501 al (1982). See text for explanation.
502
503
504 **References**
505
506 Barberi, F., Cioni, R., Rosi, M., Santacroce, R., Sbrana, A., Vecci, R., 1989. Magmatic and
507 phreatomagmatic phases in explosive eruptions of Vesuvius as deduced by grain-
508 size and component analysis of the pyroclastic deposits. J. Volcanol. Geotherm. Res.
509 38, 287–307. doi:10.1016/0377-0273(89)90044-9
510 Bardot, L., 2000. Emplacement temperature determinations of proximal pyroclastic
511 deposits on Santorini, Greece, and their implications. Bull. Volcanol. 61, 450–467.
512 doi:10.1007/PL00008911
513 Bardot, L., McClelland, E., 2000. The reliability of emplacement temperature estimates
514 using palaeomagnetic methods: A case study from Santorini, Greece. Geophys. J.
515 Int. 143, 39–51. doi:10.1046/j.1365-246X.2000.00186.x
516 Branney, M. J., & Kokelaar, B. P. (2002). Pyroclastic density currents and the
517 sedimentation of ignimbrites. Geological Society of London. Special Publication.
518 Carey, S., Sigurdsson, H., 1987. Temporal variations in column height and magma
519 discharge rate during the 79 A.D. eruption of Vesuvius. Geol. Soc. Am. Bull. 99, 303–
520 314. doi:10.1130/0016-7606(1987)99<303
521 Caricchi, C., Vona, A., Corrado, S., Giordano, G., Romano, C., 2014. 79AD Vesuvius PDC
522 deposits' temperatures inferred from optical analysis on woods charred in-situ in the
523 Villa dei Papiri at Herculaneum (Italy). J. Volcanol. Geotherm. Res. 289, 14–25.
524 doi:10.1016/j.jvolgeores.2014.10.016
525 Cioni, R., Marianelli, P., Sbrana, A., 1990. L'eruzione del 79 d.C.: Stratigrafia dei depositi

ed impatto sugli insediamenti romani nel settore orientale e meridionale del Somma-Vesuvio. R. St. Pomp. IV, 179–198.

Cioni, R., Marianelli, P., Sbrana, A., 1992. Dynamics of the A.D. 79 eruption: stratigraphic, sedimentological and geochemical data on the successions from the Somma-Vesuvius southern and eastern sectors. Acta Vulcanol. 2, 109–123.

Cioni, R., Sbrana, A., Gurioli, L., 1996. The deposits of AD 79 eruption. In: Santacroce, R., et al. (Eds.), Vesuvius Decade Volcano. Workshop Handbook. Cons. Nac. Ric, Rome, Italy, pp.E1–E31.

Cioni, R., Gurioli, L., Sbrana, A., Vougioukalakis, G.E., 2000a. Precursor to the Plinian Eruptions of Threra (Late Bronze Age) and Vesuvius (AD 79): Data from Archeological Areas. Phys. Chem. Earth Part A 25, 719–724.

Cioni, R., Gurioli, L., Sbrana, A., Vougioukalakis, G.E., 2000b. Precursory phenomena and destructive events related to the Late Bronze Age Minoan (Thera, Greece) and AD 79 (Vesuvius, Italy) Plinian eruptions; inferences from the stratigraphy in the archaeological areas, in: McGuire, W.G., Griffiths, D.R., Hancock, P.L., Stewart, I.S. (Eds.), The Archaeology of Geological Catastrophes. Geological Society, London, Special Publications, 171, pp. 123–141.

Cioni, R., Gurioli, L., Lanza, R., Zanella, E., 2004. Temperatures of the A.D. 79 pyroclastic density current deposits (Vesuvius, Italy). J. Geophys. Res. 109, B02207. doi:10.1029/2002JB002251

Dioguardi, F., & Dellino, P. (2014). PYFLOW: A computer code for the calculation of the impact parameters of Dilute Pyroclastic Density Currents (DPDC) based on field data. *Computers & Geosciences*, *66*, 200-210.

Eychenne, J., Pennec, J.-L., Troncoso, L., Gouhier, M., Nedelec, J.-M., 2012. Causes and consequences of bimodal grain-size distribution of tephra fall deposited during the August 2006 Tungurahua eruption (Ecuador). Bull. Volcanol. 74, 187–205.

552 doi:10.1007/s00445-011-0517-5
553 Eppelbaum, L., Kutasov, I., & Pilchin, A. (2014). Thermal properties of rocks and density of
554 fluids. In Applied geothermics (pp. 99-149). Springer Berlin Heidelberg.
555 Guidobaldi, M.P., Esposito, D., Formisano, E., 2009. L'insula I, l'insula nord occidentale e
556 la villa dei Papiri di Ercolano: una sintesi delle conoscenze alla luce delle recenti
557 indagini archeologiche. In: Serra, Fabrizio (Ed.), Vesuviana Vol.1, 43–180.
558 Gurioli, L., Cioni, R., Sbrana, A., Zanella, E., 2002. Transport and deposition of pyroclastic
559 density currents over an inhabited area: the deposits of the AD 79 eruption of
560 Vesuvius at Herculaneum , Italy. Sedimentology 49, 929–953.
561 Gurioli, L., Houghton, B.F., Cashman, K. V, Cioni, R., 2005. Complex changes in eruption
562 dynamics during the 79 AD eruption of Vesuvius. Bull. Volcanol. 67, 144–159.
563 doi:10.1007/s00445-004-0368-4
564 Gurioli, L., Zanella, E., Pareschi, M.T., Lanza, R., 2007. Influences of urban fabric on
565 pyroclastic density currents at Pompeii (Italy): 1. Flow direction and deposition. J.
566 Geophys. Res. 112, B05213. doi:10.1029/2006JB004444
567 Jenkins, S., Komorowski, J.C., Baxter, P.J., Spence, R., Picquout, A., Lavigne, F., Surono,
568 2013. The Merapi 2010 eruption: An interdisciplinary impact assessment
569 methodology for studying pyroclastic density current dynamics. J. Volcanol.
570 Geotherm. Res. 261, 316–329. doi:10.1016/j.jvolgeores.2013.02.012
571 Kent, D. V, Ninkovich, D., Pescatore, T., Sparks, R.S.J., 1981. Palaeomagnetic
572 determination of emplacement temperature of Vesuvius AD 79 pyroclastic deposits.
573 Nature 290, 393–396.
574 Lavallée, Y., Wadsworth, F.B., Vasseur, J., Russell, J.K., Andrews, G.D.M., Hess, K.-U.,
575 von Aulock, F.W., Kendrick, J.E., Tuffen, H., Biggin, A.J., Dingwell, D.B., 2015.
576 Eruption and emplacement timescales of ignimbrite super-eruptions from thermo-
577 kinetics of glass shards. Front. Earth Sci. 3, 1–11. doi:10.3389/feart.2015.00002

578 Lesti, C., Porreca, M., Giordano, G., Mattei, M., Cas, R.A.F., Wright, H.M.N., Folkes, C.B.,
579 Viramonte, J., 2011. High-temperature emplacement of the Cerro Galán and
580 Toconquis Group ignimbrites (Puna plateau, NW Argentina) determined by TRM
581 analyses. Bull. Volcanol. 73, 1535–1565. doi:10.1007/s00445-011-0536-2
582 Lirer, L., Pescatore, T., Booth, B., Walker, G.P.L., 1973. Two plinian pumice-fall deposits
583 from Somma-Vesuvius, Italy. Geol. Soc. Am. Bull. 84, 759–772.
584 Mastrolorenzo, G., Petrone, P.P., Pagano, M., Incoronato, A., Baxter, P.J., Canzanella, A.,
585 Fattore, L., 2001. Herculaneum victims of Vesuvius in ad 79. Nature 410, 769–70.
586 doi:10.1038/35071167
587 McClelland, E.A., Druitt, T.H., 1989. Palaeomagnetic estimates of emplacement
588 temperatures of pyroclastic deposits on Santorini, Greece. Bull. Volcanol. 51, 16–27.
589 Paterson, G.A., Roberts, A.P., Mac Niocaill, C., Muxworthy, A.R., Gurioli, L., Viramonté,
590 J.G., Navarro, C., Weider, S., 2010. Paleomagnetic determination of emplacement
591 temperatures of pyroclastic deposits: an under-utilized tool. Bull. Volcanol. 72, 309–
592 330. doi:10.1007/s00445-009-0324-4
593 Pensa, A., Porreca, M., Corrado, S., Giordano, G., Cas, R., 2015a. Calibrating the pTRM
594 and charcoal reflectance (Ro%) methods to determine the emplacement temperature
595 of ignimbrites: Fogo A sequence, S??o Miguel, Azores, Portugal, as a case study.
596 Bull. Volcanol. 77. doi:10.1007/s00445-015-0904-4
597 Pensa, A., Giordano, G., Cas, R.A.F., Porreca, M., 2015b. Thermal state and implications
598 for eruptive styles of the intra-Plinian and climactic ignimbrites of the 4.6 ka Fogo A
599 eruption sequence, São Miguel, Azores. Bull. Volcanol. 77, 99. doi:10.1007/s00445-
600 015-0983-2
601 Porreca, M., 2004. Applicazioni di metodi paleomagnetici per lo studio della messa in
602 posto di flussi piroclastici. Il caso delle unita` vulcaniche recenti del cratere di Albano
603 (Italia Centrale), Ph.D. thesis, 118 pp., Univ. of Roma Tre, Rome.

604 Scott, A.C., Glasspool, I.J., 2005. Charcoal reflectance as a proxy for the emplacement
605 temperature of pyroclastic flow deposits. Geology 33, 589–592.
606 doi:10.1130/G21474.1
607 Sigurdsson, H., Cashdollar, S., Sparks, R.S.J., 1982. The Eruption of Vesuvius in A. D. 79:
608 Reconstruction from Historical and Volcanological Evidence. Am. J. Archaeol. 86, 39–
609 51.
610 Sigurdsson, H., Carey, S., Cornell, W., Pescatore, T., 1985. The eruption of Vesuvius in
611 A.D. 79. National Geographic Research 1, 332–387.
612 Sulpizio, R., Zanella, E., Macías, J. L., & Saucedo, R. (2015). Deposit temperature of
613 pyroclastic density currents emplaced during the El Chichón 1982 and Colima 1913
614 eruptions. *Geological Society, London, Special Publications*, *396*(1), 35-49.
615 Tema. E., Zanella, E., Pavon-Carrasco, F.J., Kondopoulou, D., Pavlides, S., 2015.
616 Palaeomagnetic analysis on pottery as indicator of the pyroclastic flow deposits
617 temperature: new data and statistical interpretation from the Minoan eruption of
618 Santorini, Greece. Geophys. J. Int. 203, 33-47.
619 Thomas, R.M.E., Sparks, R.S.J., 1992. Cooling of tephra during fallout from eruption
620 columns. Bull. Volcanol. 54, 542–553.
621 Turcotte, D. L., & Schubert, G. (2014). *Geodynamics*. Cambridge University Press.
622 Willcock, M.A.W., Cas, R.A.F., 2014. Primary welding and crystallisation textures
623 preserved in the intra-caldera ignimbrites of the Permian Ora Formation, northern
624 Italy: Implications for deposit thermal state and cooling history. Bull. Volcanol. 76, 1–
625 16. doi:10.1007/s00445-014-0819-5
626 Wilson, L., Sparks, R.S.J., Huang, T.C., Watkins, N.D., 1978. The Control of Volcanic
627 Column Heights by Eruption Energetics and Dynamics. J. Geophys. Res. 83, B4.
628 Wohletz, K., 2008, KWare geological software, 10 July 2008:
629 http://www.ees1.lanl.gov/Wohletz/ Heat.htm (November 2008).

Yokoyama, T., Marturano, A., 1997. Volcanic products of the Vesuvius eruption in AD79 at Pompeii, Italy. Opus. Pomp. 1–32.

Zanella, E., Gurioli, L., Pareschi, M.T., Lanza, R., 2007. Influences of urban fabric on pyroclastic density currents at Pompeii (Italy): 2. Temperature of the deposits and hazard implications. J. Geophys. Res. 112, B05214. doi:10.1029/2006JB004775

Zanella, E., Sulpizio, R., Gurioli, L., Lanza, R., 2014. Temperatures of the pyroclastic density currents deposits emplaced in the last 22 kyr at Somma-Vesuvius (Italy). Geol. Soc. London, Spec. Publ. doi:10.1144/SP396.4

Zijderveld, J. D. A. (1967). AC demagnetization of rocks: analysis of results. *Methods in paleomagnetism*, *1*, 254-286.

Figure
Click here to download high resolution image

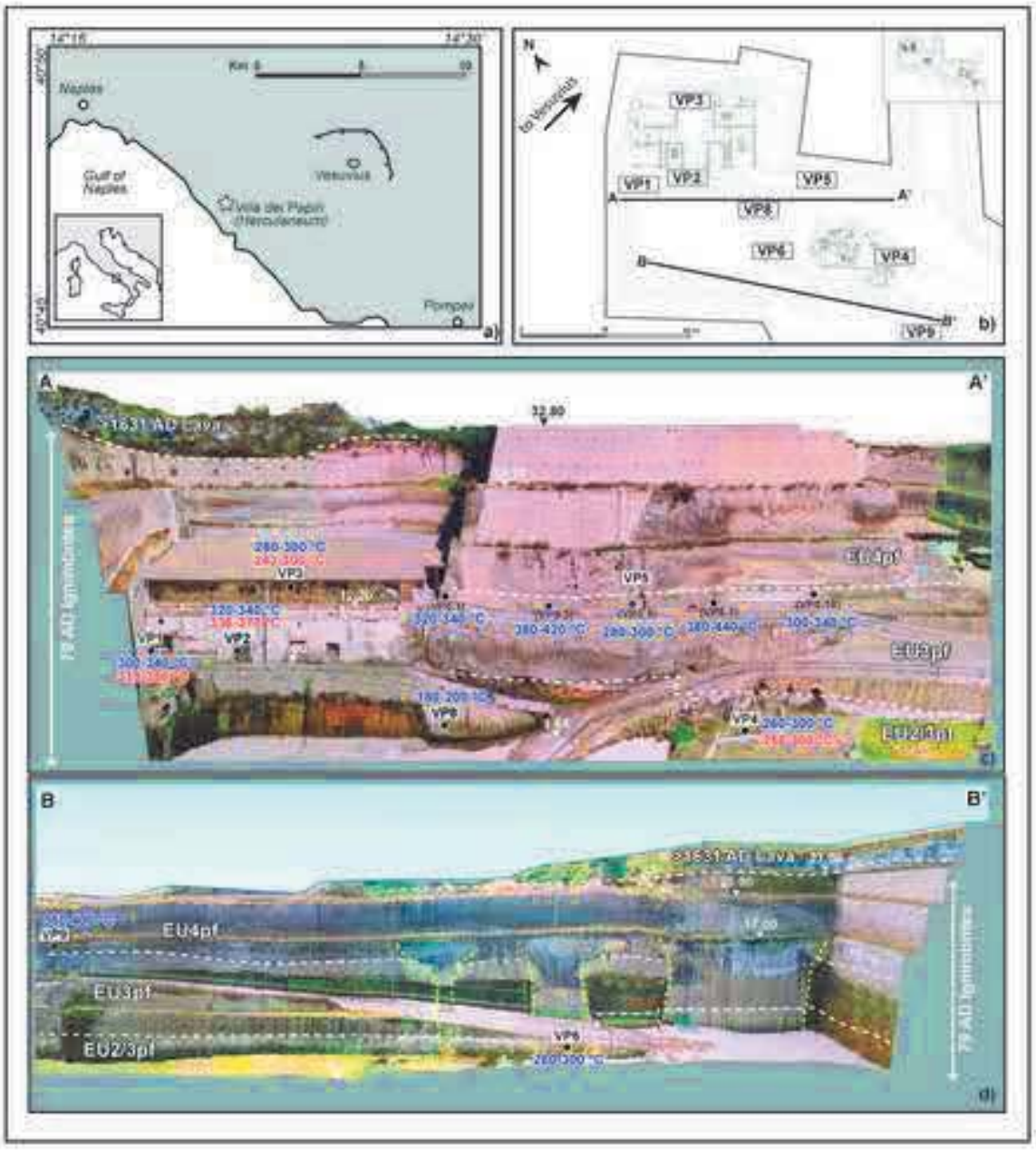

Figure
Click here to download high resolution image

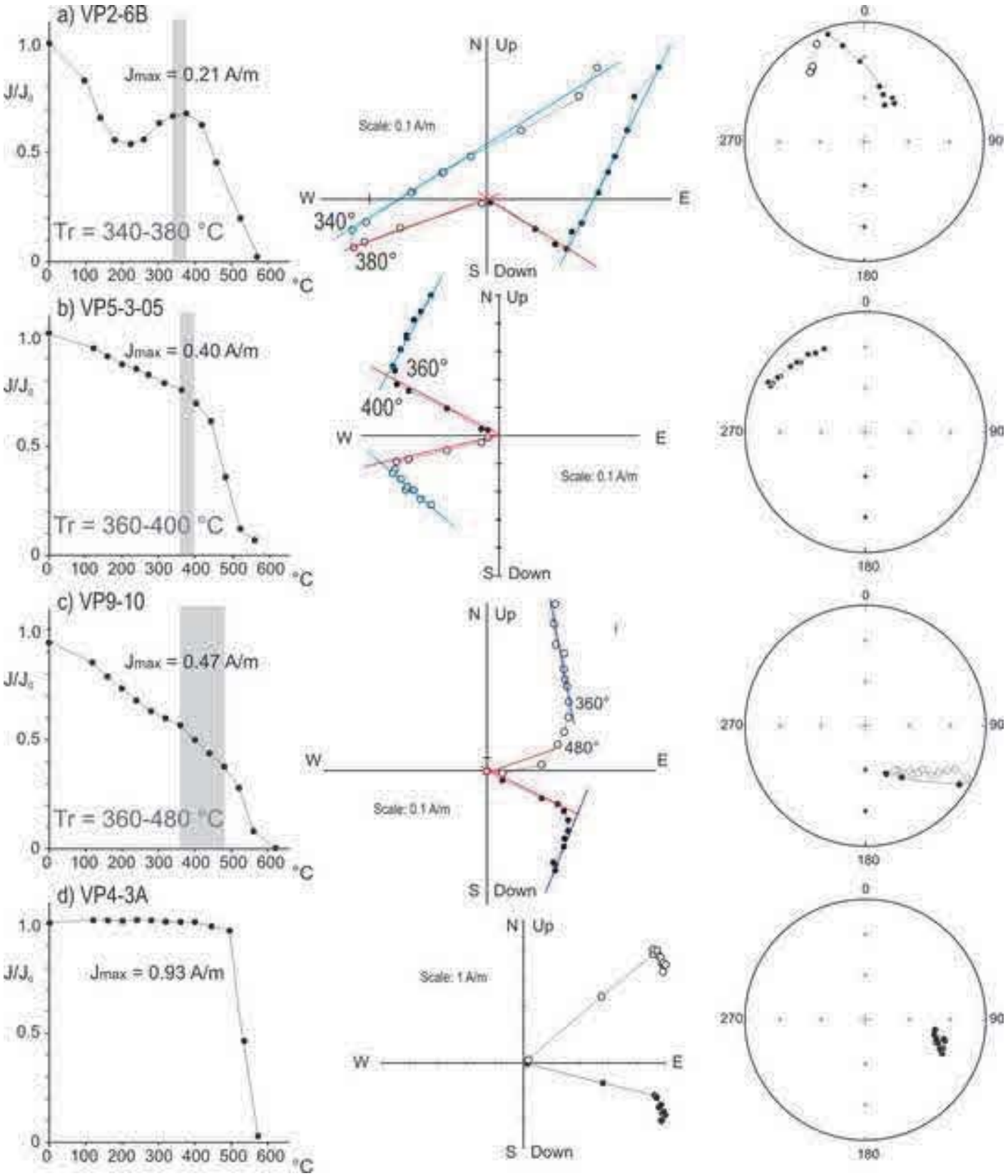

Figure
Click here to download high resolution image

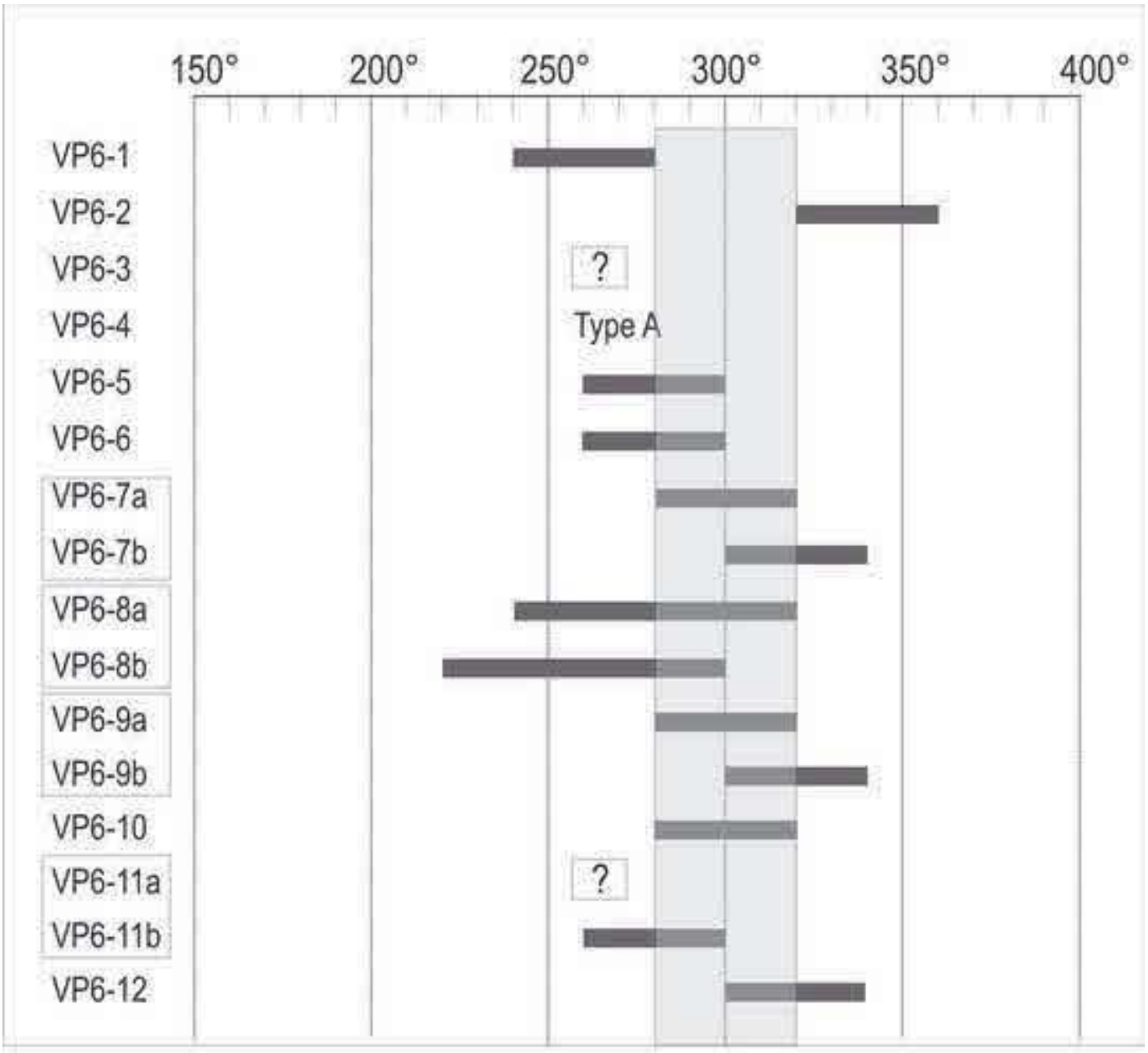

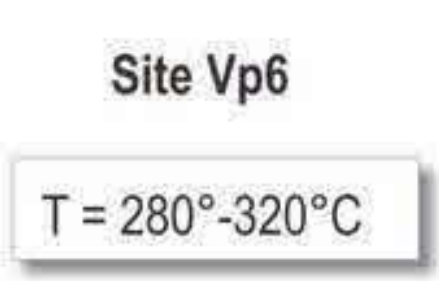

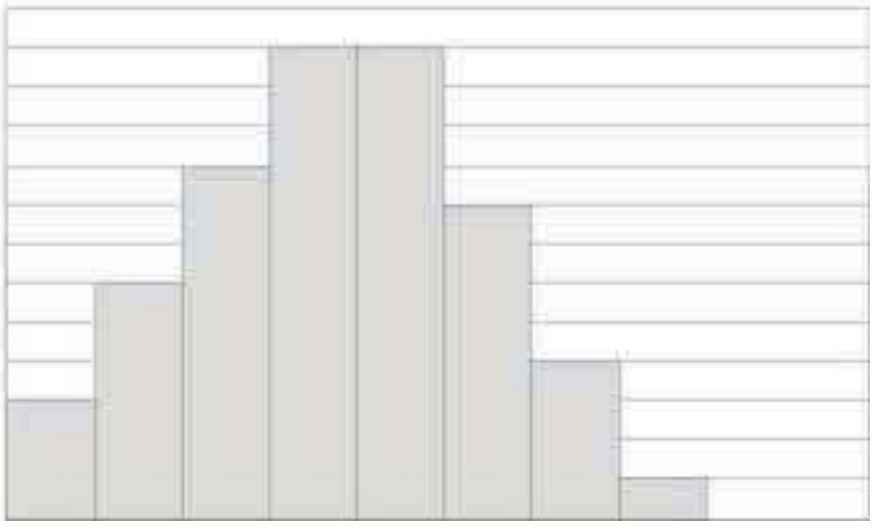

Figure
Click here to download high resolution image

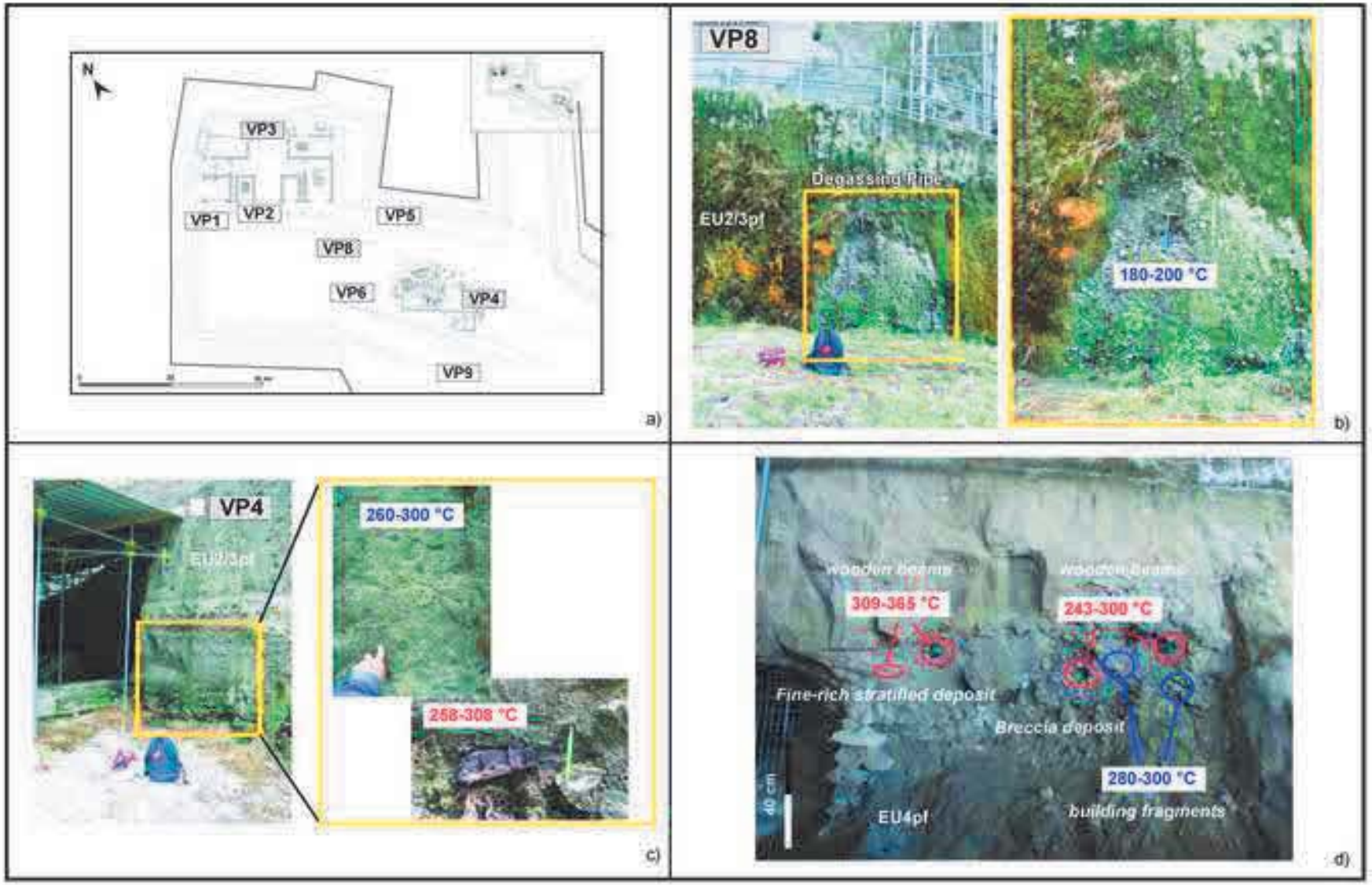

Figure
Click here to download Figure: Figure_5.pdf

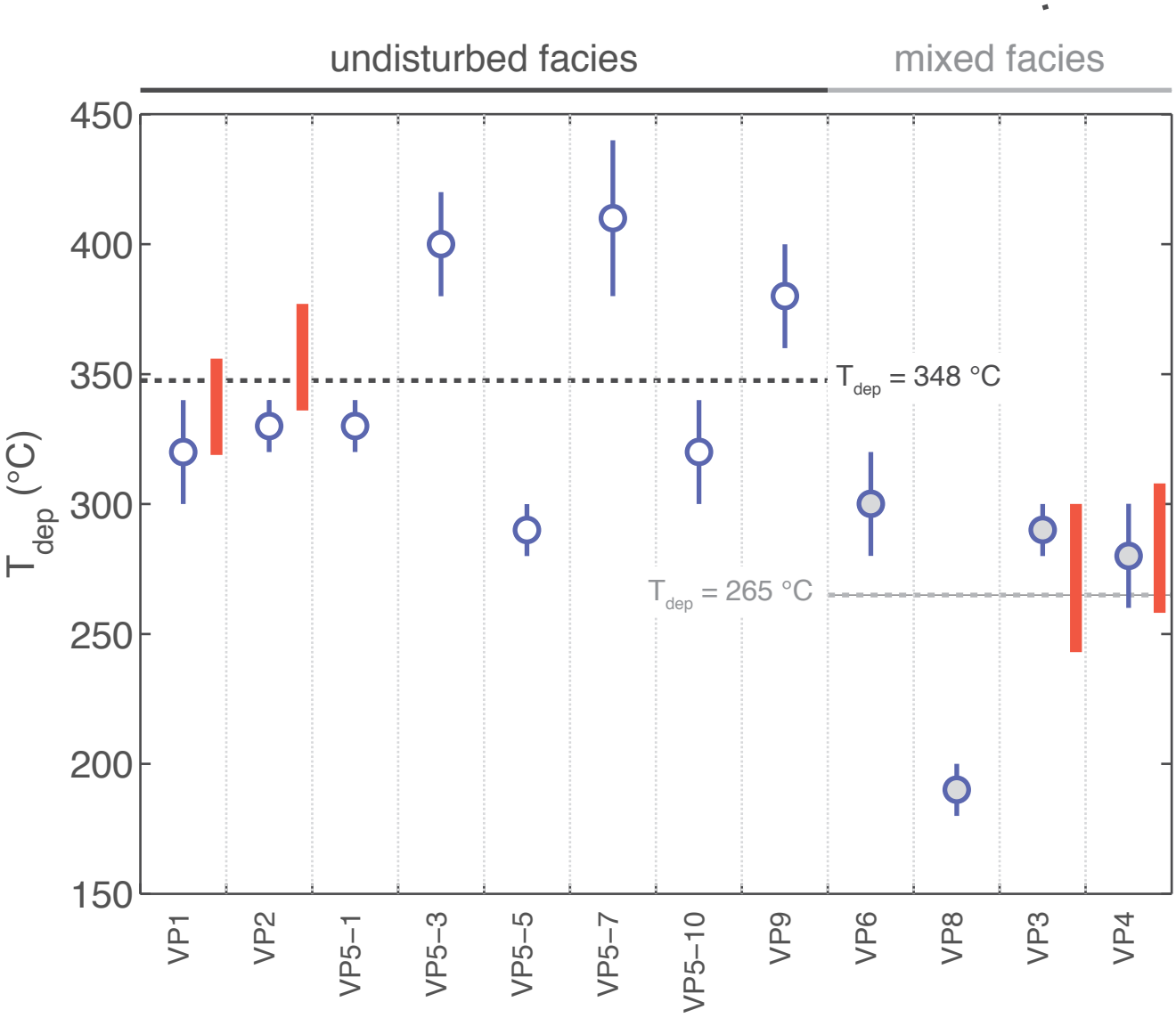

Figure

Click here to download Figure: Figure_6.pdf

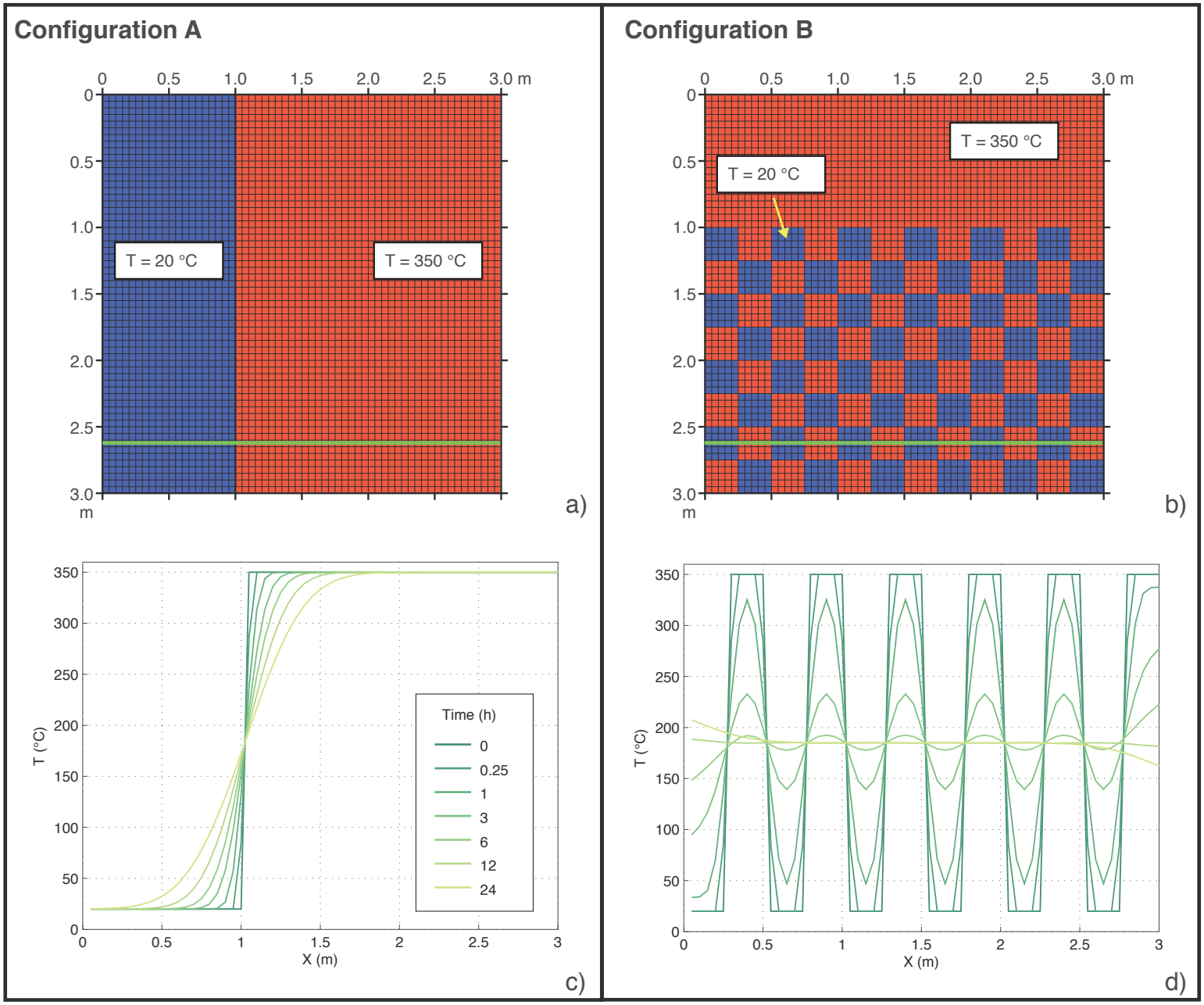

Figure

Click here to download Figure: Figure_7.pdf

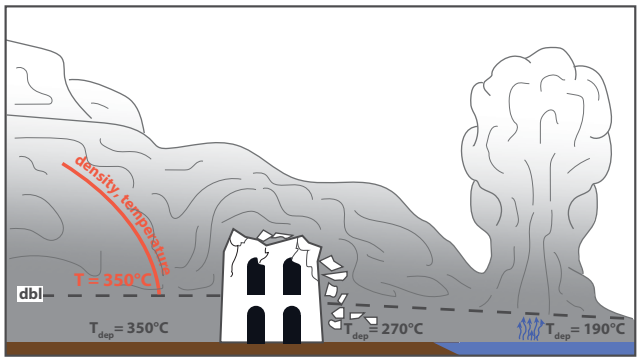

Figure
Click here to download high resolution image

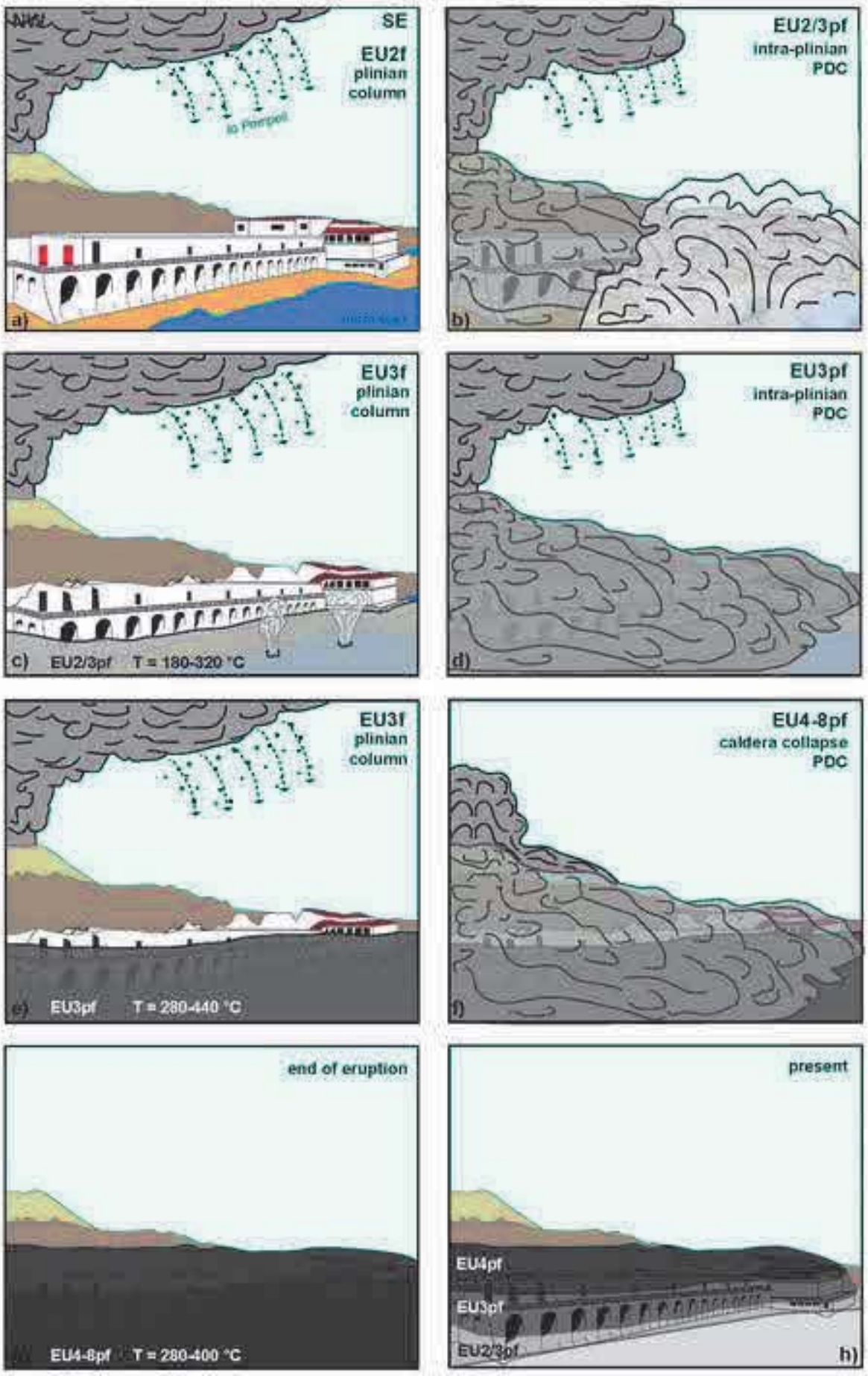

Figure (high-resolution)
Click here to download Figure (high-resolution): Figure_1_HR.pdf

Figure (high-resolution)
Click here to download Figure (high-resolution): Figure_4_HR.pdf

Figure (high-resolution)
Click here to download Figure (high-resolution): Figure_8_HR.pdf

Table
Click here to download Table: Table 1.pdf

Table 1. Results of paleomagnetic analysis.

Eruption Unit[a]	Site	n/N	Type					T_{dep}(°C)	T_{dep}charcoal (°C)[b]	Notes
			A	B	C	D	?			
	VP9	3/14	-	-	6	1	7	360-400	-	Unconsolidated lapilli tuff
EU4pf	VP3	10/12	1	1	7	1	2	280-300	243-300	Mixed debris-lapilli tuff breccia
		-	-	-	-	-	-	-	309-365	Fine-rich stratified deposit
	VP5-10	13/16	2	1	9	2	2	300-340	-	Unconsolidated lapilli tuff
	VP5-7	4/11	-	-	2	7	2	380-440	-	Unconsolidated lapilli tuff
	VP5-5	9/16	3	-	9	2	2	280-300	-	Unconsolidated lapilli tuff
EU3pf	VP5-3	7/13	1	-	7	2	3	380-420	-	Unconsolidated lapilli tuff
	VP5-1	9/16	-	3	10	3	-	320-340	-	Unconsolidated lapilli tuff near undisturbed wall
	VP2	10/16	-	1	14	1	-	320-340	336-377	Unconsolidated lapilli tuff near undisturbed wall
	VP1	9/28	2	--	14	2	10	300-340	319-356	Unconsolidated lapilli tuff near undisturbed wall
	VP6	14/16	1	-	11	2	2	280-320	-	Zeolitized lapilli tuff
EU2/3pf	VP8	10/16	-	-	14	-	2	180-200	-	Lithic rich gas pipe
	VP4	10/16	2	-	9	1	4	260-300	258-308	Mixed debris-lapilli tuff breccia

[a]According to Cioni et al. (2004);[b]T derived from charcolized woods by Caricchi et al. (2014)

Table

Click here to download Table: Table 2 physical properties.pdf

Foglio1

	initial T (°C)	density (kg/m3)	thermal conductivity (W/m-K)	Specific Heat (J/kg K)
ignimbrite	350	1200	0,7	1200
wall	20	2000	1	980

Supplementary material for online publication only

Click here to download Supplementary material for online publication only: Appendix 1, 3.doc

Supplementary material for online publication only

Click here to download Supplementary material for online publication only: Appendix 2.pdf